elements are adopted, pinned in correspondence of the slab–steel girder interface, having properties suitably calibrated to assure a translational stiffness equal to the one used in the previous applications. A pictorial view of the developed model is reported in Figure 12.

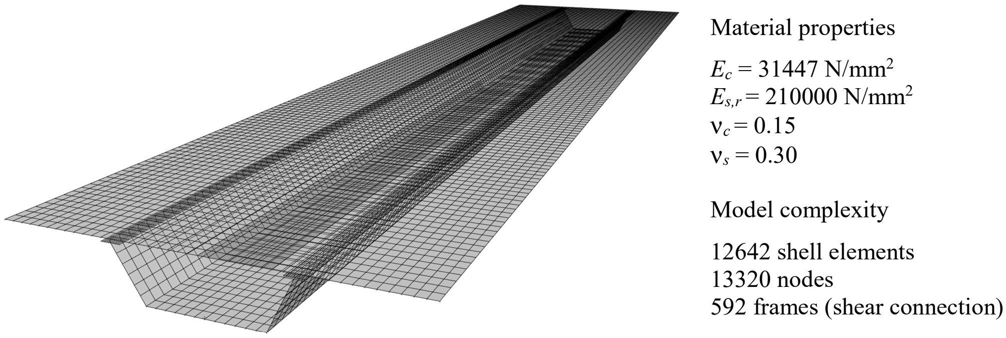

Figure 12. 3D finite element (FE) model.

Figure 13 shows the vertical deflection v_0, the slab–girder interface slip Γ_z, and the longitudinal displacements of the upper ($w_{s,sup}$) and bottom flanges ($w_{s,inf}$) of the steel girder obtained for case studies *S2-UDL*, *S3-CL*, *S2-SS*, and *S3-PW*. The results obtained considering the different beam elements (*GFE*, *CIFE*, and *IIFE*) are reported with lines of different colours and are compared with those achieved by the refined 3D FE model, represented by black dots.

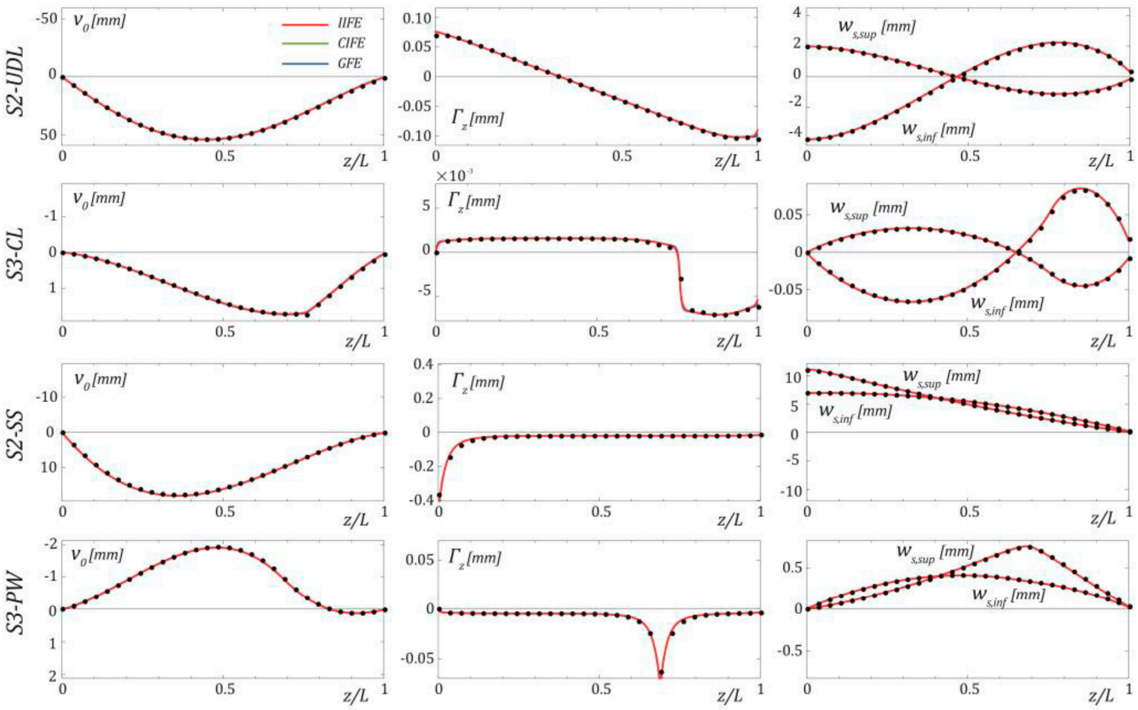

Figure 13. Comparison between the proposed beam model and the refined 3D FE model for some case studies in terms of vertical displacement v_0; interface slip Γ_z; and the longitudinal displacement of the steel girder bottom and upper flanges, $w_{s,inf}$ and $w_{s,sup}$.

Concerning the proposed beam model, a suitable number of elements is considered, on the basis of the previous applications, to assure the analysis convergence and accuracy. In detail, 200, 100, and 50 elements are considered for the *GFE*, the *CIFE*, and the *IIFE*, respectively. It can be observed that the results from the proposed beam finite elements are practically superimposed and all perfectly match the solution achieved with the refined 3D FE model.

Figure 14 compares the normal stresses on the concrete slab mid plane, on the steel girder web, and on the steel girder bottom flange obtained from the proposed beam model with those resulting from the refined 3D FE model, for case study *S2-UDL*. As the results from the beam models are almost superimposed, for the sake of simplicity, only those relevant to the *IIFE* are reported in red. The results from the refined FE model are reported with black lines. Because the response of the slab is symmetric with respect to the longitudinal middle axis, comparisons between the beam and shell finite element models are made by dividing the plot of Figure 14a into two parts, and by presenting the distribution of stresses for half of the slab.

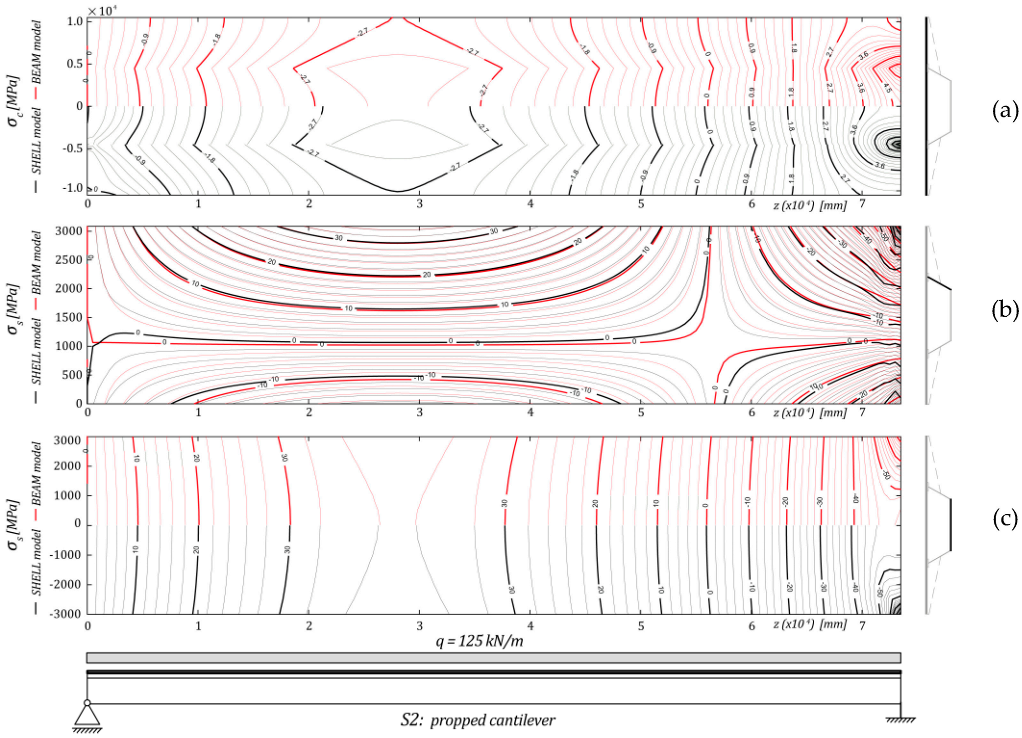

Figure 14. (**a**) Longitudinal normal stress on the slab mid plane, (**b**) on the steel girder web, and (**c**) on the steel girder bottom flange for case study *S2-UDL*.

The beam model is able to capture very well the slab normal stresses with very few differences in the bridge deck section characterised by the maximum positive bending moment and at the fixed support. Comparisons of normal stresses in the box-girder web are presented in Figure 14b by superimposing the results from the beam and shell models; normal stresses obtained by the shell model are closely reproduced with minor differences at the fixed support and in correspondence of the bridge deck section in which the overall bending moment passes from hogging to sagging. Finally, normal stresses in the bottom flange of the box-girder are compared in Figure 14c, adopting the strategy used for the concrete slab; even in this case, the beam model performs very well, furnishing results superimposed to those of the shell model.

Figure 15 compares the normal stresses on the slab mid plane, on the steel girder web, and on the steel girder bottom flange for case study *S3-CL*. As for the concrete slab (Figure 15a) and the box-girder bottom flange (Figure 15c), normal stresses of the refined shell model are closely reproduced with very small differences in the neighborhood of the applied concentrated load. Normal stresses acting on the web of the steel girder are more sensitive to the concentrated load and significant differences are observed between the proposed beam model and the refined 3D FE model (Figure 15b).

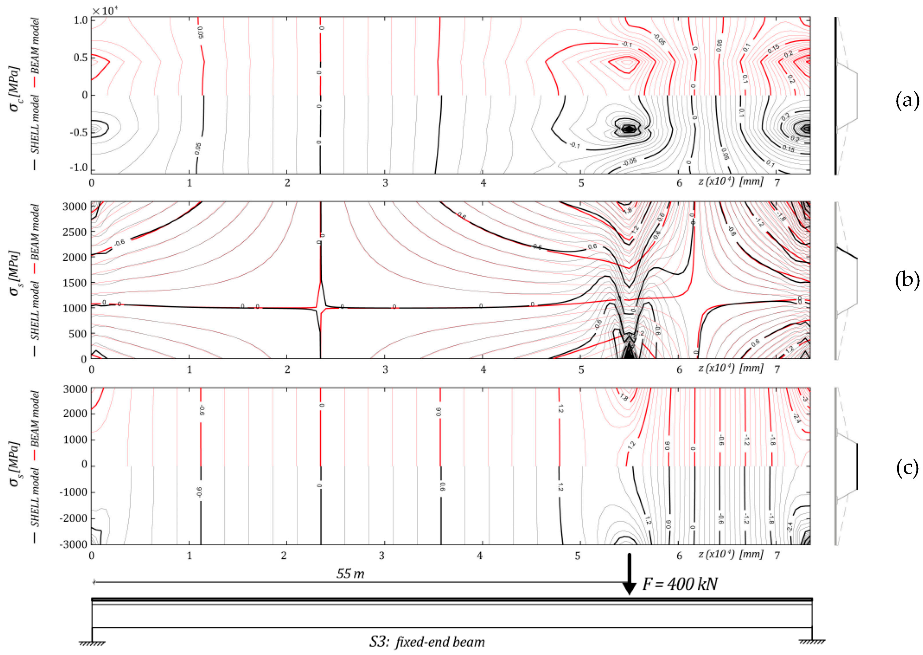

Figure 15. (**a**) Longitudinal normal stress on the slab mid plane, (**b**) on the steel girder web, and (**c**) on the steel girder bottom flange for case study *S3-CL*.

Figure 16 compares the same response parameters for case study *S2-SS*. Stresses in the concrete slab (Figure 16a) and the box-girder bottom flange (Figure 16c) resulting from the refined 3D FE model are well reproduced, with exception of only the bridge deck sections near the supports, particularly the pinned one. However, it should be remarked that stresses vanish at the pinned support, thus differences are of limited significance. Normal stresses on the web of the steel girder predicted with the proposed beam model are in very good agreement with those of the shell model, with minor discrepancies near the supports (Figure 16b).

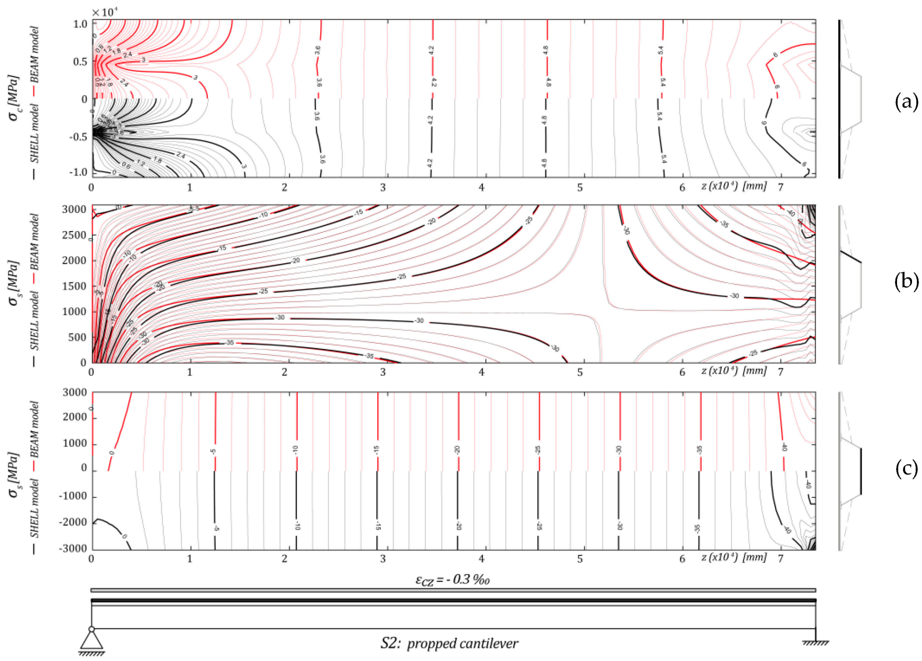

Figure 16. (**a**) Longitudinal normal stress on the slab mid plane, (**b**) on the steel girder web, and (**c**) on the steel girder bottom flange for case study *S2-SS*.

Finally, Figure 17 refers to case study *S3-PW*. Stresses in the concrete slab (Figure 17a) and the box-girder bottom flange (Figure 17c) obtained from the refined shell model are well reproduced, except for the bridge deck section subjected to the local effects induced by the pre-stressing. Normal stresses on the web of the steel girder are also well captured, even in the region affected by the pre-stressing local actions (Figure 17b).

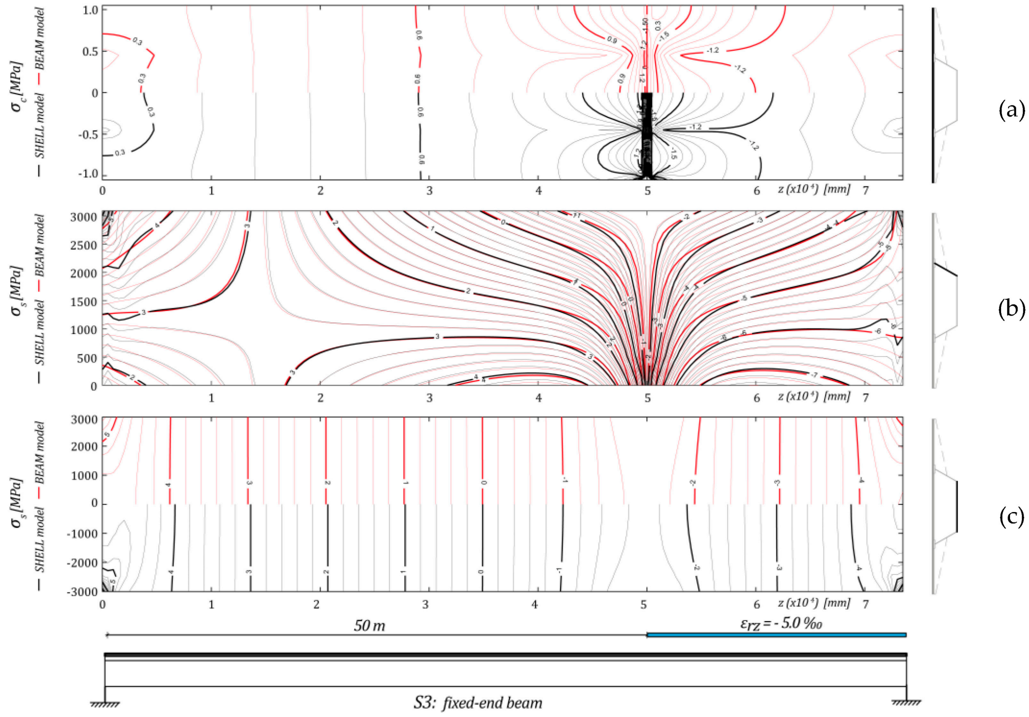

Figure 17. (**a**) Longitudinal normal stress on the slab mid plane, (**b**) on the steel girder web, and (**c**) on the steel girder bottom flange for case study *S3-PR*.

5. Conclusions

Finite elements for a higher order steel–concrete composite beam model were presented in this paper. The model, which is particularly suitable for the analysis of bridge decks, includes the partial interaction between concrete and steel members and accounts for the overall shear deformability and the shear-lag phenomenon, which strongly characterise the response of both steel and concrete elements.

Finite elements characterised by different interpolating functions are developed, implementing linear, polynomial, and exponential shape functions; the latter are derived from an analytical solution that exploits exponential matrices. The performance of the presented finite elements is investigated in terms of the solution convergence rate with reference to realistic steel–concrete composite beams with different restraints and loading conditions. The efficiency of the proposed finite elements in providing a reliable prediction of the structural response of composite beams is also addressed through comparison of the results with those achieved with a refined 3D numerical model developed using conventional shell finite elements.

The following remarks can be drawn:

- The finite element based on linear shape functions (*GFE*) suffers from locking problems and requires a highly refined discretization to reach an accurate solution of the problem;
- The finite element implementing cubic and quadratic polynomial shape functions (*CIFE*) avoids locking problems and is characterised by a higher converge rate than that based on linear shape functions (*GFE*);
- The finite element with exponential shape functions (*IIFE*) is the most performant and furnishes an almost exact solution, independent of the beam discretization, provided

that enough finite elements are adopted to avoid issues in the numerical evaluation of the exponential matrix;

- The *CIFE* is highly competitive with respect to the *IIFE*, especially in predicting beam displacements and rotations; in some cases, if very accurate solutions are not required, the former may provide results with a lower number of finite elements than that necessary to avoid instabilities in the computation of the exponential shape functions of the *IIFE*;
- In the case of distributed or concentrated loads, the convergence rate relevant to warping intensities of the steel components is much lower than that relevant to the other response parameters; differences in the convergence rate attenuate in the cases of prestressing or concrete shrinkage.

Provided that a proper discretization of the beam axis is used, depending on the adopted finite element, the beam model is able to capture very well the structural response of composite beams subjected to different loads and restraint conditions obtained from a refined 3D model. In particular, both displacements, stresses, and stress resultants of the 3D model are reproduced by the proposed beam model, which foresees a number of dofs about thirty times lower.

Author Contributions: Conceptualization, G.L. and F.G.; methodology, G.L., F.G., and S.C.; software, F.G. and S.C.; validation, G.L. and F.G.; formal analysis, G.L., F.G., and S.C.; data curation, S.C.; writing—original draft preparation, F.G. and S.C.; writing—review and editing, G.L. and F.G.; visualization, F.G. and S.C.; supervision, L.D. All authors have read and agreed to the published version of the manuscript.

Funding: This research received no external funding.

Data Availability Statement: The data presented in this study are available on request from the corresponding author.

Conflicts of Interest: The authors declare no conflict of interest.

Appendix A

Stress Resultants and Inertial Components

The complete (i.e., non-compact) form of balance conditions (17), which includes stress resultants of the beam components as well as external stresses and forces, assumes the form

$$\begin{aligned}\int_0^L \left[(\boldsymbol{F}_c+\boldsymbol{F}_r)\cdot\hat{\boldsymbol{w}}_c' + \boldsymbol{S}_{cx}\cdot\hat{\boldsymbol{w}}_c + \boldsymbol{S}_{cy}\cdot\hat{\boldsymbol{w}}_c + \boldsymbol{F}_s\cdot\hat{\boldsymbol{w}}_s' + \boldsymbol{S}_{s\xi}\cdot\hat{\boldsymbol{w}}_s + V\,\hat{v}_0'\right] dz \;+\; \int_0^L q\,(\hat{\boldsymbol{w}}_s\cdot\overline{\boldsymbol{a}}_s - \hat{\boldsymbol{w}}_c\cdot\overline{\boldsymbol{a}}_c)dz \\ = \int_0^L (\boldsymbol{p}_{cz}\cdot\hat{\boldsymbol{w}}_c \;+\; \boldsymbol{p}_{sz}\cdot\hat{\boldsymbol{w}}_s \;+\; p_y\cdot\hat{v}_0)dz \;+\; (\boldsymbol{P}_{czff}\cdot\hat{\boldsymbol{w}}_c \;+\; \boldsymbol{P}_{szff}\cdot\hat{\boldsymbol{w}}_s \;+\; P_{ya}\cdot\hat{v}_0)|_{\alpha=0,L}\end{aligned} \tag{A1}$$

where

$$\boldsymbol{F}_c = \int_{A_c} \sigma_{cz}\,\boldsymbol{a}_c\,dA = \begin{bmatrix} N_c \\ M_c \\ W_c \end{bmatrix} \tag{A2}$$

$$\boldsymbol{S}_{cx} = \int_{A_c} \tau_{cxz}\,\boldsymbol{a}_{c,x}\,dA = \begin{bmatrix} 0 \\ 0 \\ Q_{cx} \end{bmatrix} \tag{A3}$$

$$\boldsymbol{S}_{cy} = \int_{A_c} \tau_{cyz}\,\boldsymbol{a}_{c,y}\,dA = \begin{bmatrix} 0 \\ V_c \\ 0 \end{bmatrix} \tag{A4}$$

$$\boldsymbol{F}_r = \int_{A_r} \sigma_{rz}\,\boldsymbol{a}_c\,dA = \begin{bmatrix} N_r \\ M_r \\ W_r \end{bmatrix} \tag{A5}$$

$$\boldsymbol{F}_s = \sum_{i=1}^{n} t_i \int_0^{l_i} \sigma_{sz}\, \boldsymbol{a}_s\, d\xi_i = \begin{bmatrix} N_s \\ M_s \\ W_{sy} \\ W_{sx} \end{bmatrix} \tag{A6}$$

$$\boldsymbol{S}_{s\xi} = \sum_{i=1}^{n} t_i \int_0^{l_i} \tau_{s\xi z}\, \boldsymbol{a}_{s,\xi}\, d\xi_i = \begin{bmatrix} 0 \\ V_s \\ Q_{sy} \\ Q_{sx} \end{bmatrix} \tag{A7}$$

$$\boldsymbol{S}_{s\xi} = \sum_{i=1}^{n} t_i \int_0^{l_i} \tau_{s\xi z}\, \boldsymbol{a}_{s,\xi}\, d\xi_i = \begin{bmatrix} 0 \\ V_s \\ Q_{sy} \\ Q_{sx} \end{bmatrix} \tag{A8}$$

are the generalized stress resultants,

$$\boldsymbol{p}_{cz} = \int_{A_c \,\cup\, A_r} b_z\, \boldsymbol{a}_c\, dA + \int_{\partial A_c \,\cup\, \partial A_r} s_z\, \boldsymbol{a}_c\, dl = \begin{bmatrix} q_{cz} \\ m_{cx} \\ \omega_{cy} \end{bmatrix} \tag{A9}$$

$$\boldsymbol{p}_{cz} = \int_{A_c \,\cup\, A_r} b_z\, \boldsymbol{a}_c\, dA + \int_{\partial A_c \,\cup\, \partial A_r} s_z\, \boldsymbol{a}_c\, dl = \begin{bmatrix} q_{cz} \\ m_{cx} \\ \omega_{cy} \end{bmatrix} \tag{A10}$$

$$q_y = \int_{A_c \,\cup\, A_r} b_y\, dA + \int_{\partial A_c \,\cup\, \partial A_r} s_y\, dl + \sum_{i=1}^{n} t_i \int_0^{l_i} \mathrm{b_y}\, d\xi_i + \sum_{i=1}^{n} \int_0^{l_i} \mathrm{s_y}\, \mathrm{dl} \tag{A11}$$

are the resultants of forces applied along the beam, and

$$\boldsymbol{P}_{cz\alpha} = \int_{(A_c \,\cup\, A_r)_\alpha} s_z\, \boldsymbol{a}_c\, dA = \begin{bmatrix} F_{cz\alpha} \\ M_{cx\alpha} \\ W_{cy\alpha} \end{bmatrix} \qquad con\ \alpha = 0, L \tag{A12}$$

$$\boldsymbol{P}_{sz\alpha} = \int_{(A_s)_\alpha} s_z\, \boldsymbol{a}_s\, dA = \begin{bmatrix} F_{sz\alpha} \\ M_{sx\alpha} \\ W_{sx\alpha} \\ W_{sy\alpha} \end{bmatrix} \qquad con\ \alpha = 0, L \tag{A13}$$

$$Q_{y\alpha} = \int_{(A_c \,\cup\, A_r)_\alpha} s_y\, dA + \int_{(A_s)_\alpha} s_y\, dA \qquad con\ \alpha = 0, L \tag{A14}$$

are the resultants of the forces applied at the beam end cross sections. Inertia of the beam cross section, constituting the global stiffness matrix $\boldsymbol{K}$, is

$$\boldsymbol{I}_c = \int_{A_c} \boldsymbol{a}_c \otimes \boldsymbol{a}_c\, dA \tag{A15}$$

$$\boldsymbol{J}_c = \int_{A_c} \boldsymbol{a}_{c,x} \otimes \boldsymbol{a}_{c,x} + \boldsymbol{a}_{c,y} \otimes \boldsymbol{a}_{c,y}\, dA \tag{A16}$$

$$\boldsymbol{L}_c = \int_{A_c} \boldsymbol{a}_{c,y}\, dA \tag{A17}$$

$$\boldsymbol{I}_r = \int_{A_r} \boldsymbol{a}_c \otimes \boldsymbol{a}_c\, dA \tag{A18}$$

$$\boldsymbol{I}_s = \sum_{i=1}^{n} t_i \int_0^{l_i} \boldsymbol{a}_s \otimes \boldsymbol{a}_s\, d\xi_i \tag{A19}$$

$$\boldsymbol{J}_s = \sum_{i=1}^{n} t_i \int_0^{l_i} \boldsymbol{a}_{s,\xi} \otimes \boldsymbol{a}_{s,\xi}\, d\xi_i \tag{A20}$$

$$\boldsymbol{L}_s = \sum_{i=1}^{n} t_i \int_0^{l_i} \boldsymbol{a}_{s,\xi}\, y_{,\xi}\, d\xi_i \tag{A21}$$

$$m_s = \sum_{i=1}^{n} t_i \int_0^{l_i} y_{,\xi}^2\, d\xi_i \tag{A22}$$

$$\boldsymbol{A}_{\alpha\beta} = \overline{\boldsymbol{a}}_\alpha \otimes \overline{\boldsymbol{a}}_\beta \qquad \alpha, \beta = c,\ s \tag{A23}$$

Appendix B

Stress State

Stresses of Equations (9)–(11), relevant to strains descending from the admissible displacement field according to constitutive relationships, are usually referred to as active stresses and can be used to compute normal longitudinal stresses σ_{cz}, σ_{sz}, and σ_{rz} with negligible errors (Equations (9)–(11)). However, active stresses do not satisfy the local equilibrium, which also requires additional non-vanishing stress components, called reactive stresses. The latter do not appear in the virtual work theorem expression and can be estimated by means of the local equilibrium conditions. These components are significant in the case of shear stresses. By assuming concrete and steel members as thin-walled elements, the total shear stresses τ_{cxz} and $\tau_{s\xi z}$ may be calculated separately for the concrete slab and the steel girder, starting from the local equilibrium. For the steel girder, by considering the constitutive law in Equation (10), the local equilibrium condition with null body forces provides

$$\sigma'_{sz} + \tau_{s\xi z,\ \xi} = 0 \tag{A24}$$

which, integrated along the local curvilinear abscissa ξ, yields

$$\tau_{s\xi z}(\xi, z) = \widetilde{\tau}_{s\xi z} - \mathrm{E_s}\, \boldsymbol{w}''_s \int_0^{\xi} \boldsymbol{a}_s d\xi + \mathrm{E_s} \int_0^{\xi} \overline{\varepsilon}'_{sz}\, d\xi \tag{A25}$$

Equation (A25) is valid for each wall of the steel girder; $\widetilde{\tau}_{s\xi z}$ is an integration constant that has to be evaluated by imposing equilibrium conditions at the wall edges. As for the concrete slab, reinforcements are assumed to be smeared within the slab so that shear stress discontinuities only occur at the slab–girder connection. Thus, the slab is divided into different panels, each one characterised by a curvilinear abscissa ξ and by the relevant shear stresses $\tau_{c\xi z}$. The local equilibrium condition is provided by the following relationship:

$$\int_{h_c} \sigma'_{cz} dy + \int_{h_r} \sigma'_{rz}\, dy + \tau_{c\xi z,\ \xi}\, h_c = 0 \tag{A26}$$

where h_c is the thickness of the slab and h_r is the notional thickness of the smeared reinforcements. By considering constitutive laws in Equation (9) and Equation (11), integration along the local abscissa ξ yields

$$\begin{aligned} \tau_{c\xi z}(\xi, z) = \widetilde{\tau}_{c\xi z} \quad & -\tfrac{1}{h_c}\mathrm{E}_c\, \boldsymbol{w}''_c \textstyle\int_0^{\xi} \int_{h_c} \boldsymbol{a}_c d\xi dy + \tfrac{1}{h_c}\mathrm{E_c} \int_0^{\xi} \int_{h_c} \overline{\varepsilon}'_{cz}\, d\xi dy \\ & -\tfrac{1}{h_c}\mathrm{E}_r\, \boldsymbol{w}''_c \textstyle\int_0^{\xi} \int_{h_r} \boldsymbol{a}_c d\xi dy + \tfrac{1}{h_c}\mathrm{E_r} \int_0^{\xi} \int_{h_r} \overline{\varepsilon}'_{rz} d\xi dy \end{aligned} \tag{A27}$$

where, analogously to the steel girder, $\widetilde{\tau}_{s\xi z}$ is an integration constant that has to be evaluated by imposing equilibrium conditions at the wall edges.

Appendix C

Notations

The following symbols are used in this paper:

0	origin of Cartesian coordinate system;
$\boldsymbol{A}$	matrix containing stiffnesses of the beam cross section;
A	area;
$\boldsymbol{a}$	geometric vector;
$\boldsymbol{B}$	matrix containing stiffnesses of the beam cross section;
$\boldsymbol{b}$	vector of the integration constants;
B	concrete slab width;
$\boldsymbol{C}$	matrix containing stiffnesses of the beam cross section;
$\boldsymbol{c}$	vector of loads and stress-independent strain along the beam;
$\boldsymbol{d}$	vector of all unknown displacements;
d	differential operator;
$\boldsymbol{E}$	exponential matrix;
E	Young's modulus;
$\boldsymbol{f}$	vector of nodal forces;
f_c, f_{sh}, f_{sv}	warping intensity functions;
G	shear modulus;
h_c	slab thickness;
$\boldsymbol{I}$	inertia matrix or identity matrix;
$\boldsymbol{J}$	inertia matrix;
$\boldsymbol{K}$	stiffness matrix of the beam element;
k, i	indexes;
L	length of the beam;
l	length of the beam plane walls;
l_e	length of the finite element;
$\boldsymbol{L}$	inertia matrix;
M	bending moment at the beam end cross section;
m	bending moment along the beam axis;
N	longitudinal force at the beam end cross section;
$\boldsymbol{N}_e$	matrix of interpolating functions;
$\bar{\boldsymbol{n}}$	vector of resultants of forces due to restrained stress-independent strain;
n	number of the plane steel walls;
n_e	number of finite elements
$\boldsymbol{p}$	resultants of external forces along the beam axis;
$\boldsymbol{P}$	resultants of external forces at the beam end cross section;
Q_v	resultant of vertical loads at the beam end cross section;
q_c, q_s	longitudinal forces along the beam axis;
q_v	resultant of vertical loads along the beam axis;
$\boldsymbol{R}$	inverse of matrix of exponential matrices evaluated at beam ends;
$\boldsymbol{s}$	vector grouping unknown displacements and their first derivative;
t_i	thickness of the *i*-th plane steel wall;
$\cup$	linear matrix operator;
$\boldsymbol{U}$	displacement of the two end cross sections of the beam;
$\boldsymbol{u}$	displacement of the end cross section of the beam;
u	transverse displacement, along coordinate direction X;
$\boldsymbol{v}_e$	vector of the unknown nodal displacements;
$\boldsymbol{v}$	assembled vector of the nodal displacements of all the elements;
v	vertical displacement of the cross section, along coordinate direction Y;
W	bi-moment at the beam end cross section;
w	longitudinal displacement, along coordinate direction Z;
$\boldsymbol{w}$	vector grouping the generalised displacements;
X, Y, Z	coordinate axes;
x, y, z	coordinates;
$\bar{x}$, $\bar{y}$	coordinates of the slab–girder interface connection;
α	direction cosine of the local abscissa;

ϵ, k, μ	overall stress-independent strain;
$\bar{\boldsymbol{\varepsilon}}$	vector of stress-independent strains;
$\bar{\varepsilon}$	stress-independent strain;
$\widetilde{\varepsilon}$	generic nonlinear stress-independent longitudinal strain field;
Φ	rotation;
Γ	beam–slab interface slip;
η	local abscissa of the finite element;
λ	normalised abscissa of the finite element
μ	interpolating function;
ν	Poisson's ratio; interpolating function
ρ	stiffness per-unit-length of the shear connection;
σ_z	normal stress;
τ	shear stress;
υ	interpolating function;
ω	bi-moment along the beam axis;
ξ	local abscissa of the beam plane walls;
ψ_c	slab warping function;
ψ_{sh}	steel warping function due to longitudinal shear flow;
ψ_{sv}	steel warping function due to shear force.
Subscripts	
c	concrete part of the composite beam;
e	finite element;
r	steel reinforcement part of the composite beam;
s	steel part of the composite beam;
0	referred to the origin of coordinate system;
,	partial derivatives.
Symbols and Superscripts	
T	concrete part of the composite beam;
$'$	derivative with respect to z variable;
$\mathcal{D}$	formal linear differential operator;
$\hat{}$	variation;
$\cdot$	scalar product.

References

1. European Committee for Standardization (CEN). *Eurocode 4: Design of Composite Steel and Concrete Structures–Part 2: Rules for Bridges*; EN1994-2; CEN: Brussels, Belgium, 2005.
2. Newmark, N.M.; Siess, C.P.; Viest, I.M. Test and analysis of composite beams with incomplete interaction. *Proc. Soc. Exp. Stress Anal.* **1951**, *9*, 75–92.
3. Nguyen, Q.H.; Hjiaj, M.; Uy, B. Time-dependent analysis of composite beams with partial interaction based on time-discrete exact stiffness matrix. *Eng. Struct.* **2010**, *32*, 2902–2911. [CrossRef]
4. Ranzi, G.; Bradford, M.A. Analysis of composite beams with partial interaction using the direct stiffness approach accounting for time effects. *Int. J. Numer. Methods Eng.* **2009**, *78*, 564–586. [CrossRef]
5. Gara, F.; Ranzi, G.; Leoni, G. Time analysis of composite beams with partial interaction using available modelling techniques: A comparative study. *J. Constr. Steel Res.* **2006**, *62*, 917–930. [CrossRef]
6. Dezi, L.; Gara, F.; Leoni, G. Construction sequence modelling for continuous steel-concrete composite decks. *Steel Compos. Struct.* **2006**, *6*, 123–138. [CrossRef]
7. Gara, F.; Leoni, G.; Dezi, L. Slab cracking control in continuous steel-concrete bridge decks. *J. Bridge Engrg. ASCE* **2013**, *18*, 1319–1327. [CrossRef]
8. Ranzi, G.; Bradford, M.A. Nonlinear analysis of composite beams with partial shear interaction by means of the direct stiffness method. *Steel Compos. Struct.* **2009**, *9*, 131–158. [CrossRef]
9. Virtuoso, F.; Vieira, R. Time dependent behaviour of continuous composite beams with flexible connection. *J. Constr. Steel Res.* **2004**, *60*, 451–463. [CrossRef]
10. Dall'Asta, A.; Zona, A. Three-field mixed formulation for the non-linear analysis of composite beams with deformable shear connection. *Finite Elem. Anal. Des.* **2004**, *40*, 425–448. [CrossRef]
11. Gara, F.; Ranzi, G.; Leoni, G. Displacement-based formulations for composite beams with longitudinal slip and vertical uplift. *Int. J. Numer. Methods Eng.* **2006**, *65*, 1197–1220. [CrossRef]
12. Ranzi, G.; Gara, F.; Ansourian, P. General method of analysis for composite beams with longitudinal and transverse partial interaction. *Comput. Struct.* **2006**, *84*, 2373–2384. [CrossRef]

13. Taig, G.; Ranzi, G. Generalised beam theory for composite beams with longitudinal and transverse partial interaction. *Math. Mech. Solids* **2017**, *22*, 2011–2039. [CrossRef]
14. Nguyen, Q.H.; Hjiaj, M.; Guezouli, S. Exact finite element model for shear-deformable two layer beams with discrete shear connection. *Finite Elem. Anal. Des.* **2011**, *47*, 718–727. [CrossRef]
15. da Silva, A.R.; Sousa, J.B.M. A family of interface elements for the analysis of composite beams with interlayer slip. *Finite Elem. Anal. Des.* **2009**, *45*, 305–314. [CrossRef]
16. Gara, F.; Leoni, G.; Dezi, L. A beam finite element including shear lag effect for the time dependent analysis of steel–concrete composite decks. *Eng. Struct.* **2009**, *31*, 1888–1902. [CrossRef]
17. Timoshenko, S. Theory of bending, torsion and buckling of thin walled members of open section. *J. Frankl. Inst.* **1945**, *239*, 249–268. [CrossRef]
18. Xu, R.; Wang, G. Bending solutions of the Timoshenko partial-interaction composite beams using Euler-Bernoulli solutions. *J. Eng. Mech. ASCE* **2013**, *139*, 1881–1885. [CrossRef]
19. Vo, T.P.; Thai, H.T. Static behaviour of composite beams using various refined shear deformation theories. *Comp. Struct.* **2012**, *94*, 2513–2522. [CrossRef]
20. Zona, A.; Ranzi, G. Finite element models for nonlinear analysis of steel–concrete composite beams with partial interaction in combined bending and shear. *Finite Elem. Anal. Des.* **2011**, *47*, 98–118. [CrossRef]
21. Ranzi, G.; Zona, A. A steel–concrete composite beam model with partial interaction including the shear deformability of the steel component. *Eng. Struct.* **2007**, *29*, 3026–3041. [CrossRef]
22. Schnabl, S.; Saje, M.; Turk, G.; Planinc, I. Analytical solution of two-layer beam taking into account interlayer slip and shear deformation. *J. Struct. Eng.* **2007**, *133*, 886–894. [CrossRef]
23. Dezi, L.; Gara, F.; Leoni, G.; Tarantino, M.A. Time dependent analysis of shear-lag effect in composite beams. *J. Engrg. Mech. ASCE* **2001**, *127*, 71–79. [CrossRef]
24. Dezi, L.; Gara, F.; Leoni, G. Shear-Lag effect in twin-girder composite decks. *Steel Compos. Struct.* **2003**, *3*, 111–122. [CrossRef]
25. Dezi, L.; Gara, F.; Leoni, G. Effective slab width in prestressed twin-girder composite decks. *J. Struct. Engrg. ASCE* **2006**, *132*, 1358–1370. [CrossRef]
26. Macorini, L.; Fragiacomo, M.; Amadio, C.; Izzuddin, B.A. Long-term analysis of steel–concrete composite beams: FE modelling for effective width evaluation. *Eng. Struct.* **2006**, *28*, 1110–1121. [CrossRef]
27. Gara, F.; Ranzi, G.; Leoni, G. Partial interaction analysis with shear-lag effects of composite bridges: A finite element implementation for design applications. *Adv. Steel Constr.* **2011**, *7*, 1–16.
28. Gara, F.; Ranzi, G.; Leoni, G. Analysis of the shear lag effect in composite bridges with complex static schemes by means of a deck finite element. *Int. J. Steel Struct.* **2008**, *8*, 249–260.
29. Gonçalves, R.; Camotim, D. Steel-concrete composite bridge analysis using Generalised Beam Theory. *Steel Compos. Struct.* **2010**, *10*, 223–243. [CrossRef]
30. Gara, F.; Leoni, G.; Carbonari, S.; Dezi, L. A higher order steel-concrete composite beam model. *Eng. Struct.* **2014**, *80*, 260–273. [CrossRef]
31. Chakrabarti, A.; Sheikh, A.H.; Grifith, M.; Oehlers, D.J. Analysis of composite beams with longitudinal and transverse partial interactions using higher order beam theory. *Int. J. Mech. Sci.* **2012**, *59*, 115–125. [CrossRef]
32. Computer and Structures, Inc. *CSI Analysis Reference Manual*; SAP 2000; Computer and Structures, Inc.: Berkeley, CA, USA, 2011.
33. Reddy, J.N. On locking-free shear deformable beam finite elements. *Comput. Methods Appl. Mech. Engrg.* **1997**, *149*, 113–132. [CrossRef]
34. Moler, C.; Van Loan, C. Nineteen Dubious Ways to Compute the Exponential of a Matrix, Twenty-Five Years Later. *SIAM Rev.* **2003**, *45*, 3–49. [CrossRef]